ACADEMIA ROMÂNĂ
Revue Roumaine de Chimie
http://web.icf.ro/rrch/

Rev. Roum. Chim.,
2010, *55*(7), 369-375

Fe, Ce AND Cu INFLUENCE ON MORPHO-STRUCTURAL AND PHOTOCATALYTIC PROPERTIES OF TiO_2 AEROGELS

Mihaela POPA,[a] Emil INDREA,[b] Petru PASCUȚA,[c] Veronica COȘOVEANU,[a] Ionel Catalin POPESCU[a] and Virginia DANCIU[a*]

[a]"Babes-Bolyai" University, Faculty of Chemistry and Chemical Engineering, Electrochemical Research Laboratory, 11 Arany Janos Str, Cluj-Napoca, 400028 Roumania
[b]National Institute for Research and Development of Isotopic and Molecular Technologies, Physics of Multifunctional Nanostructured Systems, 65-103 Donath Str., Cluj-Napoca, 400293 Roumania
[c]Technical University, Faculty of Materials Science and Engineering, Department of Physics, 103-105 Muncii Avenue Cluj-Napoca, 400641 Roumania

Received May 15, 2009

Fe, Ce and Cu doped TiO_2 aerogels were prepared by sol-gel method followed by supercritical drying with liquid CO_2. Samples of aerogels, containing ~1 at% metal ions, were characterized and used as catalysts for salicylic acid photodegradation, chosen as reference water pollutant. X-ray diffraction, UV-VIS spectrophotometry and BET method were used to investigate the structural and morphological peculiarities of the obtained aerogels. The photocatalytic activity of metal doped TiO_2 aerogels were compared with that of undoped one and it was found that it depends on the metal type and its concentration. Under similar experimental conditions, Ce doped TiO_2 aerogel shows the highest efficiency for salicylic acid photodegradation.

INTRODUCTION

Nowadays the environmental protection is one of the most important objectives of the humanity. A lot of techniques are employed to accomplish this task. Among these photocatalysis is a promising method used in degradation of different water or air organic pollutants. The principle of photocatalysis involves the mineralization of organic compounds till CO_2 and H_2O by using the UV-VIS irradiation of the photocatalyst.

Regarding its properties, TiO_2 is considered a very suitable photocatalyst. It is a nontoxic material, with chemical stability, low cost and high oxidation power [1]. TiO_2 is a semiconductor with a band gap of about 3.2 eV allowing absorption of UV light (about 5% of solar spectrum). However, the absorption of only a small fraction of the solar spectrum makes TiO_2 not enough efficient for practical applications. Additionally, the electron-hole recombination is considered a serious problem for its photocatalytic performances, since this process limits severally the TiO_2 quantum yield [2].

Doping TiO_2 with transition metals has been considered an efficient method for extending the TiO_2 absorption in visible region of solar spectrum [3,4]. At the same time, it was stated that doping metals create localized states in TiO_2 band gap, acting as electron/hole traps. However, the beneficial effect of metal doping is still uncertain, being sometimes accepted or rejected [5-8].

Cu doped TiO_2 xerogels has been traditionally used for CO_2 photocatalytic reduction process, but few studies were dedicated to photo-oxidation processes [9-11]. Thus, in comparison with undoped TiO_2, Cu-TiO_2 xerogels, synthesized by sol-gel process, showed an enhanced photocatalytic activity for methylene-blue photo-oxidation [11]. Ce and Fe doped TiO_2 xerogels were more frequently investigated, but their effect on the photocatalytic activity still remains a controversial subject. Thus,

* [1] Corresponding author: vdanciu@chem.ubbcluj.ro

Fe doped TiO_2 showed a higher photocatalytic activity for phenol,[6] methanol,[12] methyl orange[13] and cyclohexane[14] photodegradation, than that observed for undoped TiO_2. Similarly, Ce doped TiO_2 showed a better efficiency for formaldehyde[15] and 4-chlorophenol[16] photodegradation. In the case of TiO_2, it was found that the optimum concentration of metal doping is placed in the range of 0.5 - 1 at % [17, 18]. At the same time, it was reported that: (i) Fe doped TiO_2 decrease the TiO_2 photocatalytic activity for methylene blue[19] and benzoic acid [20] degradation; (ii) Ce doped TiO_2 presents lower photoactivity for rhodamine B [21] photodegradation than undoped TiO_2. Generally, it was concluded that the photocatalytic efficiency of metal doped TiO_2 is strongly dependent on the conditions of preparation, on their morphostructural properties (crystalline structure, specific surface area, and surface OH group's concentration) and on the type of the organic pollutant [21]. It was noticed that by incresing the specific surface area (~ 150 m^2/g) and the surface OH group's concentration, the pollutant adsorption and photodegradation efficiency on the titania based photocatalyst increase [22, 23]. Titania aerogels combine the aerogel properties (high porosity and high surface area) [24, 25] with those of the TiO_2.

The aim of this paper was to obtain Fe-, Ce-, Cu-doped TiO_2 aerogels and to investigate the influence of the type of doping metal on morpho-structural properties and on the salicylic acid photodegradation efficiency, respectively.

RESULTS AND DISCUSSION

1. X-ray diffraction

The XRD characteristics of Fe-TiO_2, Ce-TiO_2, Cu-TiO_2 (Fig. 1), and undoped TiO_2 (500°C) samples are shown in Table.1. Anatase (tetragonal $D_{4h}I4_1/amd$) was the main crystalline phase of all the investigated samples. However, brookite and rutile phases are also present. The highest amount of anatase was found in Fe doped and Ce doped TiO_2. The formation of brookite phase seems to be favoured in the undoped and Cu doped TiO_2 aerogel. The presence of Cu favours the formation of rutile phase too.

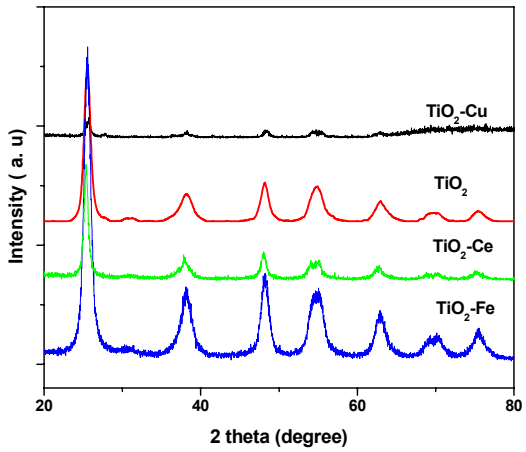

Fig. 1 – XRD patterns of the obtained aerogel samples.

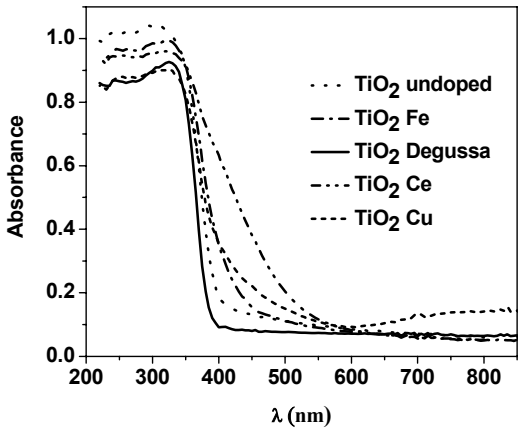

Fig. 2 – UV-vis spectra for doped, undoped TiO_2 and Degussa P25 samples.

The calculation of the cell parameters (especially the *c* parameter for the tetragonal cell) could give information about the position of the foreign metal in TiO_2 lattice [6]. The *c* value of all doped TiO_2 samples was smaller than that estimated for undoped TiO_2 sample, suggesting that the doping metal was not incorporated in TiO_2 lattice. The presence of doping metals in TiO_2 samples affects the particles size too. In Ce and Cu doped samples the value of the particles size was 1.71 times, respectively, 1.58 times higher than that for undoped TiO_2, while for Fe doped TiO_2 sample it was slightly smaller. The microstrain evolution is dominated by particles size effect. As particle size increases the microstrain decreases. On the other hand, metal introduction into the anatase lattice and the associated generation of oxygen vacancies would be expected to produce an increase in the lattice microstrain.

Table 1

Metal content determination and structural characteristic of the examined samples

Sample	Metal content[a] (%)	Structural analysis[b]						
		Anatase	Rutile	Brookite	Anatase			Microstrain $< \varepsilon^2 >^{1/2} \times 10^3$
		(%)			Particle size (nm)	Cell parameters a = b; c (Å)	Unit cell volume (Å^3)	
TiO_2	-	72.5	2.1	25.4	10.3	3.795; 9.499	136.8	3.86
Fe-TiO_2	0.72	96.3	1.2	2.5	9.6	3.790; 9.485	136.1	3.91
Ce-TiO_2	1.6	94.9	1.8	3.3	17.7	3.790; 9495	136.4	3.31
Cu-TiO_2	0.82	75.3	10.5	14.2	16.2	3.785; 9.488	135.9	3.58

[a]ICP-MS measurements; errors ± 5 %
[b]determined from XRD patterns

2. DRS measurements

The UV-VIS spectra are shown in Fig. 2. The spectrum of pure anatase TiO_2 Degussa P25 (385 nm ~3.23 eV) was considered the reference for our doped and undoped TiO_2 aerogels. The band gap values determined from diffuse reflectance spectra are presented in Table 2. Ce doped TiO_2 shows a large range of absorption in the visible region (around 525 nm), determining the biggest narrowing of the TiO_2 band gap. Cu doped TiO_2 presents absorption around 408 nm and also over 600 nm of the visible region. The band located at 400-500 nm might be assigned to three-dimensional Cu^+ clusters existing in the CuO matrix, generated by the partial reduction of Cu^{2+}. The adsorption bands at 600-800 nm are assigned to $2E_g \rightarrow 2T_{2g}$ transitions of Cu^{2+} located in the distorted or perfect octahedral symmetry, respectively [26]. Among the doped samples, Fe doped TiO_2 exhibits the smallest absorption in the visible range (around 451 nm).

3. Pore characterization

Adsorption and desorption isotherms of N_2 on the prepared samples are presented in Fig. 3. According with IUPAC classification (1985), the physiosorption isotherms of doped and undoped TiO_2 aerogels correspond to type IV with the H2 hysteresis loop. In this case, the pore structures are complex and tend to be made up of interconnected networks of pores of different size and shape [27]. The values of mean mesopore radius and cumulative pores volume are presented in Table 2. Undoped TiO_2 aerogel exhibits the highest mesopores volume, while mesopores volume of Fe-TiO_2, Ce-TiO_2 and Cu-TiO_2 was 1.46, 1.88, and, respectively, 1.40 times smaller. S_{BET} of the metal doped TiO_2 aerogels was almost unchanged in the case of Fe doped TiO_2, but it decreased 1.63 times for Ce doped TiO_2 and 1.24 times for Cu doped TiO_2. Metal doping of TiO_2 induces a decreasing of the pore volume and specific surface area.

4. Photocatalytic activity

All doped samples showed a slightly lower photocatalytic activity comparing with undoped TiO_2 (Fig. 4). Among the metal doped TiO_2 samples, the highest value of the apparent rate constant was observed for Fe doped TiO_2. This could be due to the high amount of anatase phase (96.3%), the high surface area, the smallest particles size and the biggest pore volume found for Fe doped TiO_2.

In order to estimate the effect of doping metal on the photocatalytic activity of TiO_2 aerogels, corrected for the differences existing between the S_{BET} values, the k_{app}/S_{BET} ratio was calculated. It was found that Ce doped TiO_2 exhibits the highest value of k_{app}/S_{BET} ratio. Despite of its small S_{BET} and mesopores volume, it has a high percentage of anatase (94.9 %), a high amount of OH surface groups (regarding the metal doped series) and a high mesopores radius. A high amount of anatase phase has an increasing effect on photoactivity which could compensate a low specific surface area.[28] Additionally, the OH surface groups favor the salicylic acid adsorption on the photocatalyst surface and thus the photodegradation rate will increase [29].

The area occupied by a single molecule of SA is about 0.32 nm^2 [30] and, considering a spherical shape of the molecule, the radius of SA would be 0.319 nm. The mesopores presents different shapes (as the isotherms reveals), having smaller or higher entrance diameters.

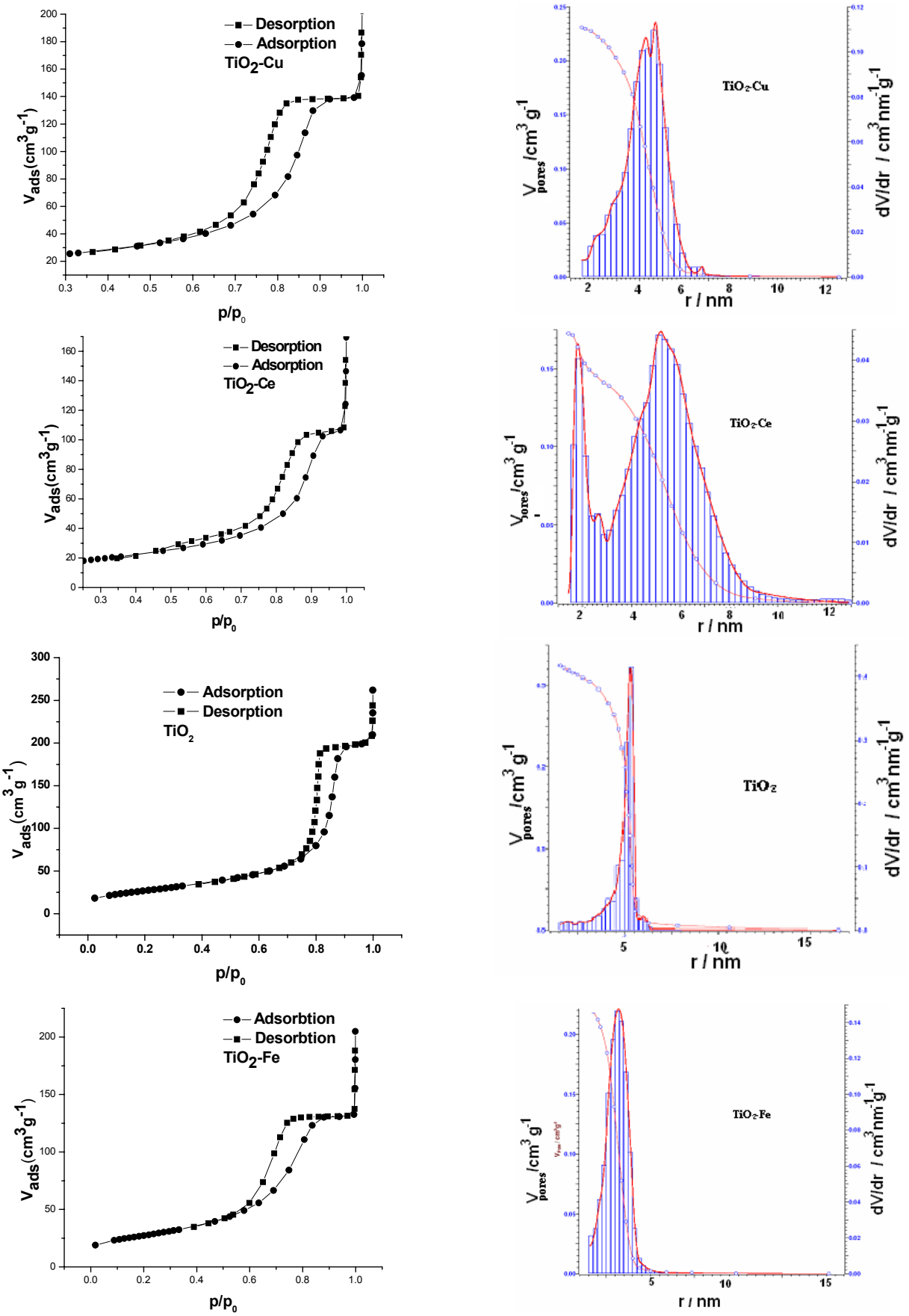

Fig. 3 – Adsorption-desorption isotherms and pores size distribution of undoped and Ce-, Fe-, Cu- doped TiO_2 aerogels.

Table 2

Electronic and structural properties and photocatalytic activity of the examined sample

Catalyst	Band gap (eV)	Pores mean radius (nm)	Pores volume (cm^3/g)	OH surface concentration (mol/m^2)	S_{BET} (m^2/g)	k_{app} (10^3 min^{-1})	k_{app} / S_{BET} (g/m^2min)	ξ (10^4)
TiO_2	3.14	5.18	0.324	0.0170	144	10.23	0.071	1.22
Fe-TiO_2	2.76	3.12	0.222	0.0077	96	9.84	0.102	1.24
Ce-TiO_2	2.37	5.1	0.172	0.0113	60	9.75	0.191	1.27
$CuTiO_2$	3.05	4.7	0.231	0.0111	79	6.89	0.087	1.00
TiO_2 Degussa	3.23	6.9[38]	-	0.011	42.3	2.50	0.047	0.55

An appropriate value of the pore entrance diameter allows the diffusion of SA molecule in the mesopores and thus the adsorption of SA molecules on the nanoparticles surface is favored. The mean mesopores radius value for Ce doped TiO_2 is about 1.63 times higher than that estimated for Fe doped TiO_2 (Table 2), indicating a better coverage with SA adsorbed molecules and, consequently, a higher hole transfer rate between catalyst and SA molecules.

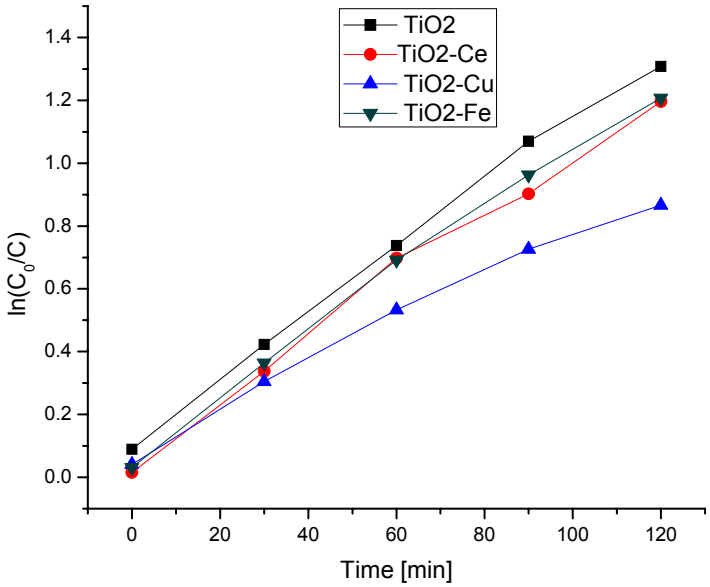

Fig. 4 – Photocatalytic activity of the obtained photocatalysts.

The lower photocatalytic activity of Cu doped TiO_2 could be attributed to the segregation of an important amount of Cu^{2+} (CuO) on the aerogel surface during the thermal treatment. Cu^{2+} species would easily uptake one photogenerated electron from the TiO_2 conduction band leading to Cu^+, and thus will decrease the number of electrons able to diffuse on the surface and to form OH·. Since no stabilization of Cu^+ ion might be considered, a subsequent reoxidation would occur by a hole trapping and Cu^{2+} will be formed [24].

Another explanation could be that the surface homogeneous distribution of Cu oxide in TiO_2 aerogel probably hinders the $OH^{\bullet}$ radical development and, additionally, blocks the adsorption centers destined to the organic compound [31].

The activity of the photocatalysts, correlated with the UV-VIS light intensity, was evaluated by determining the photonic efficiency (ξ) of SA degradation. The highest values of ξ were noticed for Ce doped TiO_2 and Fe doped TiO_2 (Table 2). In these cases it is possible that the photons are more efficient used to generate electron-hole pairs (the recombination time of the photogenerated pair could be increased), leading to a better SA photodegradation with respect of bare and Cu doped TiO_2.

EXPERIMENTAL

1. Samples preparation

For the synthesis of iron, copper and cerium doped as well as undoped TiO_2 gels were used: Ti(IV) isopropoxide (TIP)

(>98%, Merck-Schuchardt), anhydrous ethanol (EtOH) (analytical grade, Aldrich), deionised H_2O and HNO_3 (analytical grade, 70%, Primexchim), $Fe(NO_3)3{\cdot}9H2O$, $Ce(NO_3)_2{\cdot}6H_2O$, $Cu(NO_3)_2{\cdot}3H_2O$ (Aldrich). The molar ratios were H_2O: TIP = 3.75, EtOH:TIP = 21 and HNO_3:TIP = 0.1, $Me(NO_3)_x$/TIP = 0.015. The synthesis was done at room temperature, with stirring. The supercritical drying with liquid CO_2 of TiO_2 gels was performed in a critical point dryer (SAMDRI-PVT 3D, Tousimis), in the following conditions: 0.1 kg/min fill rate, 3.5 h purging time, 40 min. heat time, 1h maintained in supercritical conditions (100 atm, 40°C), 1 h depressurizing time. The obtained aerogels were thermal treated at 500°C for 2h in air, using a CARBOLITE furnace, and then were morpho-structural characterized.

2. Sample characterization

X-ray Diffraction (XRD) measurements were performed using a BRUKER D8 Advance X-Ray diffractometer, working at 45 kV and 30mA. The Cu K_α radiation, Ni filtered, was collimated with Soller slits. Pure silicon powder standard sample was used to correct the data for instrumental broadening. The microstructural information obtained by single X-ray profile Fourier analysis of TiO_2 anatase nanoparticles were the effective crystallite mean size, *D (nm)* and the root mean square (rms) of the microstrains averaged along the [*hkl*] direction, $\langle\varepsilon^2\rangle^{1/2}hkl$.[32] The Warren-Averbach X-ray profile Fourier analysis of the (1 0 1), (2 0 0) and (2 1 5) TiO_2 anatase peak profiles were processed by a XRLINE [33] computer program. Unit cell parameters were calculated through Rietveld refinement using the PowderCell software.[34] PowderCell program enables a quantitative phase (volume fractions) analysis method by comparison of the different scattering power of component materials.

UV-VIS absorption spectra of powders were performed using a Jasco V-650 spectrophotometer with integrating sphere attachment, having a diffuse reflectance in the range of 200-800 nm. Band gap energy was evaluated by extrapolating the linear part of the $(A_b\times h\nu)$ vs hν curve to the energy axis.[35]

The isotherms of the obtained samples were recorded using a Sorptomatic 1990, Thermo. Before measuring the adsorption isotherms, the calcined samples were heated at 120°C for 2 hours. The specific surface area (S_{BET}) of the samples was calculated by BET method using the N_2 adsorption. Mesopores size distribution was determined using the Barrett, Joyner and Halenda method.

Surface OH groups were spectrophotometrically determined by measuring the decreasing of iron acetilacetone [$Fe(acac)_3$ - in toluene solution] concentration after its absorption on the sample surface, according to the reaction:[36]

$$(3\text{-}x)\ \text{S-OH} + Fe(acac)_3 \rightarrow (\text{S-O})_{3-x}Fe(acac)_x + (3\text{-}x)\text{acacH}$$

where, S stands for TiO_2 surface.

Quantum yield for UV-VIS light was determined by actinometry, based on the following equation:

$$Fe(C_2O_4)_3^{3-} + h\nu \rightarrow Fe^{2+} + 2\ C_2O_4^{2-} + \text{oxidized oxalate}$$

The quantity of formed Fe^{2+} was spectrophotometrically estimated, using phenanthroline (λ = 510 nm). The intensity of the light absorbed by the system was $2.26\ 10^{-6}$ Einstein/min. The photonic efficiency of salicylic acid (SA) was determined using the following equation [37]:

$$\xi = \text{SA moles reacted per time unit / Einstein absorbed per time unit}$$

Bulk metal analysis was performed using an inductively coupled plasma-mass spectrometer (Specrophame D).

3. Photocatalytic activity

The photocatalytic activity of the doped and undoped TiO_2 aerogels was determined by monitoring the photodegradation of the salicylic acid (with a concentration of $5*10^{-4}$ M) taken as standard pollutant. Photodecomposition experiments were performed in a Teflon cell, equipped with a quartz window for UV-VIS illumination using a high pressure Hg lamp (250 W, HBO Osram).

The photodegradation profile was obtained by spectrophotometrical determination (λ = 295 nm) of the SA concentration, using a Jasco V-650 spectrophotometer. The working temperature was 20-22°C and the solution pH was 5.3. Before UV irradiation, as well as before UV-VIS measurements, the cell with the sample was kept in dark for 15 minutes in order to achieve the equilibrium of the adsorption-desorption process. To evaluate the photocatalytic activity of the doped, undoped TiO_2 aerogels and TiO_2 Degussa powder, the dependence $\ln(C_0/C)$ *vs.* time was recorded for salicylic acid. The apparent rate constant (k_{app}) (Table 2) of the salicylic acid photodegradation was taken as the slope $\ln(C_0/C)$ *vs.* time plot.

CONCLUSIONS

Iron, cooper or cerium doped as well as undoped TiO_2 aerogels were prepared. The morphological and structural properties were analyzed, using different techniques. All TiO_2 aerogel samples, the XRD analysis revealed anatase as the majority component of the crystalline structure and also the presence of brookite and rutile was detected. The size of the anatase crystallites for Ce and Cu doped samples were 1.71 and 1.58 times higher than that observed for undoped TiO_2, while for Fe doped TiO_2 was slightly smaller. For all doped investigated aerogels, the UV-VIS measurements reveal a good absorption of the visible light, and a smaller band gap than that corresponding of undoped TiO_2. The mesopores volume and S_{BET} values decreased after doping TiO_2 with transition metals. Fe-TiO_2 exhibits the highest mesopores volume and the smallest mesopores radius, while Ce exhibits the smallest mesopores volume and the highest mean pore size. The photocatalytic activity of the doped samples depends on the dopant nature and the morpho-structural properties of the sample. Fe doped TiO_2 exhibits the highest apparent rate constant and a high photonic efficiency, among the obtained aerogels. However, the best specific photocatalytic activity was attributed to Ce doped TiO_2 aerogel, having the highest photonic efficiency and the highest k_{app}/S_{BET}.

REFERENCES

1. E. Pelizzetti and N. Serpone (Eds.), "Photocatalysis, Fundamental and applications", Wiley, New York, 1989.
2. R.R. Ozer and J. L. Ferry, *Environ. Sci. Technol*., **2001**, *35*, 3242-3246.
3. T. Lopez, J.A. Moreno, R. Gomez, X. Bokhimi, J.A. Wang and H. Yee-Madeira, *J. Mater. Chem*., **2002**, *12*, 714-718.
4. Q. Yan, X. Su, Z. Huang and C. Ge, *J. European Ceramic Soc*., **2006,** *26*, 915-921.
5. Y. Xu, H. Chen, Z. Zeng and B. Lei, *Appl. Surf. Sci*., **2006**, *252*, 8565-8570.
6. C. Adan, A. Bahamonde, M. Fernandez Garcia and A. Martinez-Arias, *Appl. Cat. B: Environ.*, **2007,** *72*, 11-17.
7. M. Litter and J. Navio, *J. Photochem. Photobiol. A,* **1996**, *98,* 171-181.
8. R. Asahi and T. Morikawa, *Chem. Phys*., **2007,** *339*, 57-63.
9. A. Di Paola, E. Garcia-Lopez, S. Ikeda, G. Marci, B. Ohtani and L. Palmisano, *Catal.Today*, **2002,** *75*, 87-93.
10. H. S. Park, D. H. KIM, S.J. Kim and K. S. Lee, *J. Alloy Compd*., **2006**, *415*, 51-55.
11. E. Celik, Z. Gokcen, N. F. Ak Azem, M. Tanoglu and O.F. Emrullahoglu, *Mater. Sci. Eng. B*, **2006**, *132*, 258-265.
12. C. Wang, C. Bottcher, D. W. Bahnemann and J. K. Dohrmann, *J. Mater. Chem*, **2003**, *13*, 2322-2329.
13. S. Liu and Y. Chen, *Catal. Com*., **2009**, *10,* 894-899.
14. X. Li, P. Yue and C. Kutal, *New J. Chem*., **2003**, *27*, 1264-1269.
15. Y. Xu, H. Chen, Z. Zeng and B. Lei, *Appl. Surf. Sci*., **2006,** *252*, 8565-8570.
16. A. M. T. Silva, C. G. Silva, G. Dražić and J. L. Faria, *Catal. Today,* **2009**,*144,* 13-18.
17. Y. Xu, H. Chen, Z. Zeng and B. Lei, *Appl. Surf. Sci*., **2006**, *252*, 8565-8570.
18. T. Morikawa, Y. Irokawa and T. Ohwaki, *Appl. Catal. A*, **2006**, *314,* 123-127.
19. Z. Li, W. Shen and W. He, X. Zu, *J. Hazardous Mater*. ,**2008**, *155*, 590-594.
20. A. H. C. Chan, J. F. Porter, J Barford and C.K. Chan, *Mater. Research Soc*., **2002**, *17*, 1758-1765.
21. J. Xiao, T. Peng, R. Li, Z. Peng and Ch. Yan, *J. Solid Sate. Chem*., **2006,** *179*, 1161-1170.
22. P. Pichat, "Photocatalytic Degradation of Pollutants in Water and Air: Basic Concepts and Applications" Marcel Dekker, Inc, 2003.
23. P.K. Robertson, D. W. Bahnemann, J. M. C. Robertson, F. Wood In "Environmental Photochemistry Part II;" Springer-Verlag: Berlin 2005.
24. I.U. Arachige and S.L. Brock, *J. Am. Chem. Soc*., **2006,** *128*, 7964-1971.
25. T. Horikawa, M. Katoh and T. Tomida, *Micropor. Mesopor. Mater***, 2008**, *110*, 397-404.
26. G. Colon, M. Maicu, M.C. Hidalgo and J.A. Navio, *Appl. Cat. B: Environ*., **2006**, *67*, 41-51.
27. Rouquerol, J. Rouquerol and K. Sing, "Adsorption by powders and porous solids", Academic Press, 1999.
28. Y. Tanaka and M. Suganuma, *J. Sol-Gel Sci. Tech.*, **2002**, *22*, 83-89.
29. J. Aguado-Serrano and M.L. Rojas-Cervantes, *Micropor. Mesopor. Mat.,* **2006,** *88*, 205-213.
30. S. M. Ould-Mame, O. Zahraa and M. Bouchy, *International J. Photoenergy*, **2000**, *2,* 59-66.
31. J. M. Coronado, A.J. Maira, A. Martinez-Arias, J.C. Conesa and J. Soria, *J. Photochem. Photobiol*., **2002**, *150*, 213-221.
32. E. Indrea and A. Barbu, *Appl. Surf. Sci.,* **1996**, *106*, 498-501.
33. N. Aldea and E. Indrea, *Comput. Phys. Commun.,* **1990,** *60*, 155-159.
34. W. Kraus and G. Nolze, *J. Appl. Crystallogr*., **1996**, *29*, 301–303.
35. J. Xu, L. Li , Y.Yan , H. Wang, X. Wang, X. Fu and G. Li, *J. Colloid Interface Sci*., **2008**, *318*, 29–34.
36. J. A. Rob van Veen, F. T. G.Valtmaat and G.Jonkers, *J. Chem. Soc., Chem. Commun*., **1985**, 1656-1658.
37. O. Carp, C. L. Huisman and A. Reller, *Prog. Solid State Chem.*, **2004**, 32, 33 -177.
38. H. K. Shon, S. Vigneswaran, J. Kim and H. Ngo, *Korean J. Chem. Eng*., **2007**, *24*, 618-62.